First-principles study of spin-orbital coupling induced ferroelectricity in $NiBr_2$

Da-Wei Wu, Yong-Bo Yuan, Shuang Liu, Meng-Qiu Long,* and Yun-Peng Wang†
School of Physics and Electronics, Hunan Key Laboratory for Super-Micro Structure and Ultrafast Process, Central South University, 932 South Lushan Road, Changsha 410083, People's Republic of China

(Received 4 November 2022; revised 8 June 2023; accepted 1 August 2023; published 21 August 2023)

Two-dimensional multiferroic materials have attracted wide interest due to their intriguing physical properties and strong electromagnetic coupling. Among them, $NiBr_2$ is unique with a temperature dependent magnetic modulation vector **Q** which is linearly related to the electric polarization. In this work, we perform first-principles calculations on the $NiBr_2$ monolayer. Density functional theory calculations with appropriate Hubbard correction reproduce the electric polarization and its linear dependence on the magnitude of **Q**. The calculated polarization decreases as the Hubbard parameter U increases which enlarges the electronic band gap. Our results suggest the spin-orbital coupling effect of Br ions play a crucial role in generating the polarization. Wannier function analysis proves that the major contributor to electric polarization is the Br atomic orbitals which are strongly hybridized with Ni orbitals. The atomic position relaxation has a negligible contribution to the polarization.

DOI: 10.1103/PhysRevB.108.054429

I. INTRODUCTION

The research interest of multiferroics, i.e., the coexistence of (anti)ferromagnetism, ferroelectricity, and ferroelasticity has been extended to two-dimensional materials. The microscopic origin of the so-called type-II multiferroics [1] is the inversion symmetry breaking and the generation of electric polarization by complex magnetic ordering in the presence of certain lattice symmetry reduction [2]. Van der Waals two-dimensional multiferroic materials of type-II include $MnSe_2$, NiX_2 (X=Cl, Br, I), MnI_2, CoI_2, $Hf_2VC_2F_2$, etc.; reviews of these materials were provided in Refs. [3,4]. Theoretical models on the ferroelectricity due to noncollinear magnetism include the spin-current model (also called inverse Dzyaloshinskii-Moriya) [5,6], the spin-dependent metal-ligand *pd* hybridization model (also called the bond polarization model) [7,8], and others [2]. As a result, the magnetoelectric coupling between magnetic order and electric polarization is significant in these materials. Recently, the multiferroics was confirmed to persist in few-layer and even monolayers of NiI_2 [9,10].

A variety of vdW multiferroic materials have been investigated based on first-principles investigations; a thorough review is given in Ref. [4]. Here we confine ourselves to theoretical studies on pristine transition-metal halides [11–13]. Xiang *et al.* studied the spin-induced polarization of MnI_2 using density functional theory (DFT), including the spin-orbital coupling (SOC) effect and the Berry phase method, and proposed a general theory for the ferroelectric polarization induced by spin-spiral order [14]. DFT calculations reproduced the magnitude and directions of the polarization of MnI_2 [14,15]. Both the spiral magnetism and the SOC contribute to the electric polarization. The asymmetric charge distributions around I ions are more severe than around Mn ions [15]. The effect of ion displacements on the spin-induced polarization were also considered for both MnI_2 and NiI_2 [15,16]. The contribution of ion displacements to the polarization is on the same order of magnitude with the electronic contribution in these materials.

$NiBr_2$ is unique among these van der Waals multiferroic materials with the magnetic modulation vector varying as the temperature decreases [17]. At room temperature $NiBr_2$ crystallizes in rhombohedral structure with the $R\bar{3}m$ symmetry. $NiBr_2$ layers are stacked along the c axis and are bonded by weak van der Waals interactions. The Ni^{2+} ions ($3d^8$, $S = 1$) residing at the centers of edgesharing Br octahedrons form a triangular lattice. The cubic crystal field splits Ni-$3d^8$ orbitals to filled t_{2g} orbitals and half-filled e_g orbitals. Each Ni ion therefore has a local magnetic moment of 2 μ_B. Local magnetic moments order in a collinearly antiferromagnetic pattern below 44 K, but it turns to a cycloidal magnetic state below 23 K [17] due to the strong spin exchange frustrations [18]. The cycloidal state is characterized by the magnetic modulation vector $\mathbf{Q} = q\mathbf{a}^* + q\mathbf{b}^* + 3\mathbf{c}^*/2$ with q varying from 0 to 0.03 as the temperature decreases [17]. The reduction of q is accompanied by the enhancement in electric polarization up to 20 $\mu C/m^2$ at 5 K [17]. A theoretical study of the spin-induced ferroelectricity in $NiBr_2$ is still lacking.

In this work, we carried out systematic first-principles calculations and reproduced the experimental data of electric polarization in $NiBr_2$ in a spiral magnetic state. Our results confirm the crucial role of spin-orbital coupling effect of Br ions.

The rest of the paper is organized as follows. The details of the first-principles calculation methods are presented in

*mqlong@csu.edu.cn
†yunpengwang@csu.edu.cn

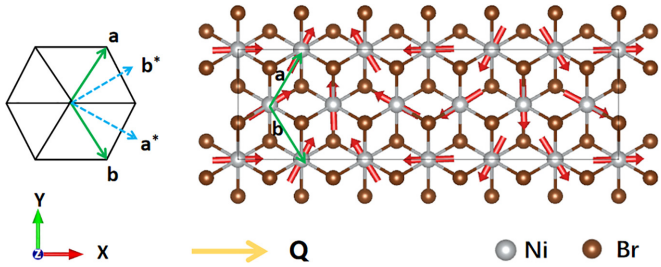

FIG. 1. The atomic structure of one supercell used in DFT calculations with $q = 1/12$. Arrows on Ni sites stand for directions of local magnetic moments. The magnetic modulation vector is $\mathbf{Q} = q\mathbf{a}^* + q\mathbf{b}^*$. The directions of lattice vectors $\mathbf{a}$, $\mathbf{b}$ and reciprocal lattice vectors $\mathbf{a}^*$, $\mathbf{b}^*$ are shown in the left inset.

Sec. II, and the results are shown in Sec. III. The conclusion is given in Sec. IV.

II. COMPUTATIONAL DETAILS

Density functional theory calculations were carried out using the Vienna *ab initio* simulation package (VASP) [19–22] and the OPENMX (open source package for material eXplorer) package [23–25]. The OPENMX code was used for distinguishing the contribution from individual atoms to the electric polarization. Utilizing an atomic orbital basis set, the OPENMX code allows setting the SOC strength of individual atomic orbitals. The atomic structure of monolayer $NiBr_2$ in the ferromagnetic state was fully optimized using VASP with the SOC effects taken into account. We also applied the Hubbard correction to the intraatomic Coulomb repulsion following both the recipes of rotationally invariant version by Liechtenstein [26] and the simplified version by Dudarev [27].

In VASP calculations, the electronic wave functions were expanded using the plane wave basis set with a kinetic energy cutoff of 500 eV. Benchmark calculations using higher cutoff energy of 500 eV give almost the same results. A uniform 7×7 k mesh was used for atomic relaxation of primitive cells until the forces on atoms were less than 10^{-3} eV/Å. Seven k points along the short edge of the supercell were used, which guarantee the convergence of both the total energy and the electric polarization.

The cycloidal state with $q = 1/2N$ was simulated using a $N \times \sqrt{3}$ supercell, (one such supercell with $q = 1/12$ is shown in Fig. 1), while the primitive cell is enough for simulating the collinear ferromagnetic state. The electric dipoles of these cycloidal supercells and that of the ferromagnetic primitive cell were computed using the Berry phase method within the modern theory of polarization [28–30]. The ferromagnetic phase preserves the inversion symmetry, thus its polarization is zero. We obtained the electric polarization after dividing their difference by the nominal volume of a monolayer. The nominal volume of the $NiBr_2$ monolayer is calculated by multiplying the area of the unit cell by the nominal thickness which is set to the calculated interlayer distance 6.13 Å. Maximally localized Wannier functions are constructed from all occupied bands using the `wannier90` code [31]. The "projections" for constructing Wannier functions are set to "`Br:s;p`" and "`Ni:d(u);dxy(d);dyz(d);dxz(d)`."

III. RESULTS

Neutron and x-ray diffraction experiments identify the magnetic modulation vector $\mathbf{Q}$ in the spin cycloidal phase of $NiBr_2$ as $\mathbf{Q} = q\mathbf{a}^* + q\mathbf{b}^* + 3\mathbf{c}^*/2$. The value of q increases as the temperature lowers and it saturates to ~0.03 at low temperatures [17]. All the magnetic moments on Ni ions are within one plane which is called the spiral plane. The spiral plane is perpendicular to the [001] direction. Neglecting the weak interlayer coupling [18], each monolayer contributes to the electric polarization independently. We considered a $NiBr_2$ monolayer in this work. The electric polarization of thick and bulk $NiBr_2$ samples can be obtained by summing up the contributions from all the monolayers. The magnetic modulation vector is expressed as $\mathbf{Q} = q\mathbf{a}^* + q\mathbf{b}^*$. Rectangular $\sqrt{3} \times n$ supercells were used for simulating the cycloidal states with $q = 1/2n$.

We first compared the relative stability of the cycloidal phase and the ferromagnetic phase. The calculated total energy difference between the two phases exhibits a minimum of -0.927 meV per Ni ion at $q = 0.12$. This result indicates that the cycloidal magnetic state is indeed more stable than the ferromagnetic state at low temperatures. Our results agree with the spin-spiral calculations of Ref. [18].

Next we turn to the electric polarization. The emergence of electric polarization generally has two origins: ionic and electronic. Electric polarization of multiferroic oxides are dominated by ionic relaxations. If this is also the case for $NiBr_2$, one would expect a stronger ionic relaxation, hence a larger ionic polarization at larger q. At the same time, a stronger ionic relaxation implies larger atomic forces in the undistorted structure. So the relation between atomic forces and the value of q is critical for examining the role played by ionic relaxations. Our DFT calculations confirm that the magnitude of atomic forces in the cycloidal phase remain nearly unchanged as the value of q increases. Therefore, ionic relaxation is not the dominant factor for electric polarization. Hereafter, we only consider the electronic part of electric polarization.

We calculated the polarization $\mathbf{P}$ of the $NiBr_2$ monolayer. The x component of $\mathbf{P}$ is exactly zero due to mirror symmetry; the z component is quite small. Fig. 2 shows the y component of the polarization P_y as a function of q with q ranging from 0.01 to 0.05. We found a nearly perfect linear dependence of the calculated P_y on q in the small-q region; the experimental data show the same linear dependence.

We find that the calculated P_y depends sensitively on the flavor and the value of the Hubbard correction. Liechtenstein's version [26] requires two parameters, namely U and J, while Dudarev's version [27] only requires one parameter denoted as U_{eff}; all parameters are in units of eV. For the case of $q = 0.025$, calculated using Liechtenstein's version with $U = 7$ and $J = 1$, P_y is equal to 20 μC/m^2, which matches the experimental data very well, see Fig. 2. The calculated P_y increases to 30 μC/m^2 when using $U = 6$, $J = 1$ and 48 μC/m^2 when using $U = 5$, $J = 1$. Using Dudarev's version, the calculated P_y is 36 μC/m^2 with $U_{\text{eff}} = 6$. As a rule of thumb, the calculated P_y shrinks by about 1.5 times as the value of U or U_{eff} increases by 1 eV.

How does the Hubbard correction affect the electric polarization? Our analysis on the cluster model indicates that

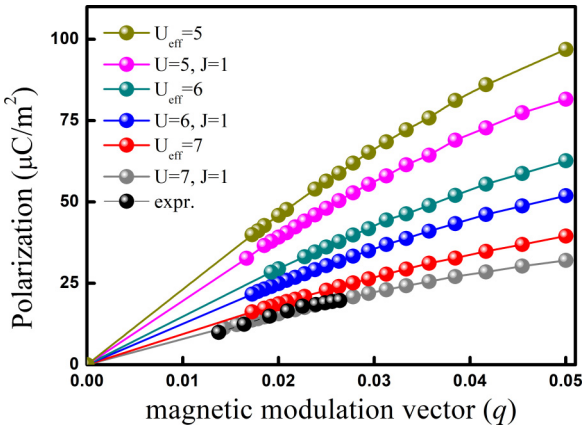

FIG. 2. The y component of electric polarization as a function of q; q defines the magnetic modulation vector as $\mathbf{Q} = q\mathbf{a}^* + q\mathbf{b}^*$. Calculation results using different flavors of Hubbard correction and the experimental data from Ref. [17] are shown as symbols. The lines are guides to eyes.

the *pd* energy difference modulates the hybridization between them, therefore the polarization is reduced as the *pd* energy difference increases. The *pd* energy difference corresponds to the electronic band gap. Based on this consideration, we calculated the band gap of $NiBr_2$ in the FM state using different Hubbard corrections. The calculated band gap increases almost linearly as the value of U or U_{eff} increases, as shown in Fig. 3(a). Plotting P_y against the band gap, we confirm the correlation between them. In Fig. 3(b), two groups of data are shown, one corresponds to $q = 0.038$ and the other to $q = 0.025$. Within each group, the calculated polarization decreases as the band gap increases.

According to the modern theory of polarization, one, in principle, cannot trace the local origin of the electronic part of the electric polarization [30]. Here let us retreat for a while and ask which atomic orbital (of Ni or Br) has dominant contribution to the polarization. In order to distinguish the contributions from Ni and Br on the electric polarization, we utilized the OPENMX code which is capable of assigning the

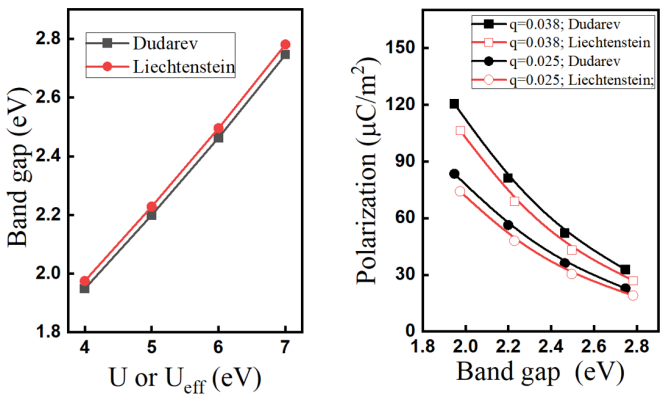

FIG. 3. (a) The dependence of calculated band gap on parameters U or U_{eff} using Liechtenstein's and Dudarev's version of Hubbard corrections. (b) The relation between electric polarization (in unit of $\mu C/m^2$) and band gap; results corresponding to two different values of q (0.038 and 0.025) are shown.

SOC strength on each atomic orbital. We did three different calculations with $q = 0.083$: (a) turning up the SOC on all Ni and Br orbitals; (b) except for Br-p orbitals, turning down the SOC on all orbitals; (c) except for Ni-d orbitals, turning down the SOC on all orbitals. Our calculations show that the electric polarization of case (b) is 308 $\mu C/m^2$ which is very close to that of (a) (263 $\mu C/m^2$). The electric polarization of (c) is only (-43 $\mu C/m^2$), which is much smaller than both (a) and (b). These results indicate that the SOC of the Br-p orbitals play a dominant role in producing the electric polarization. The contribution from Ni-d orbitals has the opposite sign with respect to Br-p orbitals, its magnitude is only about one eighth of Br-p orbitals; The sum of the two is equal to the magnitude of the electric dipole moment generated as a whole. We therefore obtain that the Ni-d and Br-p orbitals contribute to the electric polarization in an independent manner.

We also proposed a model of $NiBr_2$ in which three neighboring Ni ions and the central Br ion form a cluster. The model considers that the SOC of Br ion modulates the charge transfer between Ni and Br ions and generates a magnetic state dependent dipole momentum. After decomposing the supercell of the magnetic cycloidal state into Ni_3Br clusters, the electric polarization can be calculated, summing up the dipole moment of each cluster. The proposed cluster model is relevant to the ferroelectricity in the $NiBr_2$ monolayer. See the Supplemental Material for more details [32].

The microscopic origin of electric polarization can be analyzed using the Wannier functions. The centers of Wannier functions can be used for calculating the macroscopic electric polarization [28,29]. It is natural to associate localized Wannier functions to neighboring ions and form local dipole moments. We take the cycloidal magnetic state with the q set to $1/12$, construct the maximally localized Wannier functions, and identify the centers of Wannier functions. There are eight Wannier function centers (WFC) overlapping with each Ni ion ($d_{\uparrow}^5 d_{\downarrow}^3$), corresponding to the d orbitals of Ni ions; we associate them to the Ni ion. There are another eight Wannier functions adjacent to each Br ion (s^2p^6); their centers are depicted in Fig. 4(a). Each black sphere corresponds to two overlapping WFC's. At each Br-Ni bond, there are two WFC's which are about 0.62 Å away from the Br ion. The remaining two WFC's are on top of each Br ion with the distance of 0.44 Å. These eight Wannier functions correspond to the Br-sp orbitals with strong hybridization with Ni-d orbitals; we associate them with the Br ion.

The Ni (Br) ions together with the WFC's associated with them form Ni (Br) atoms. One can calculate the dipole moments of Ni (Br) atoms after assigning each WFC as a point charge of $-e$ and the ion as a point charge of $8e$ (e is the absolute value of electron charge). The distribution of atomic dipole moments within the supercell is shown in Figs. 4(b) and 4(c); the negligible dipole moments of Ni ions are not shown. The red arrows represent the direction of local magnetic moment of Ni ions; the blue and green arrows represent the dipole moments of Br ions above and below Ni ions. The local dipole moments are almost inplane, as indicated by the side view in Fig. 4(b). The dipole moments of Br ions above Ni is much greater than those below Ni. Across the supercell along the x direction, see Fig. 4(c), the local magnetic moments on Ni ions rotate by a period. At the same time, the electric dipole

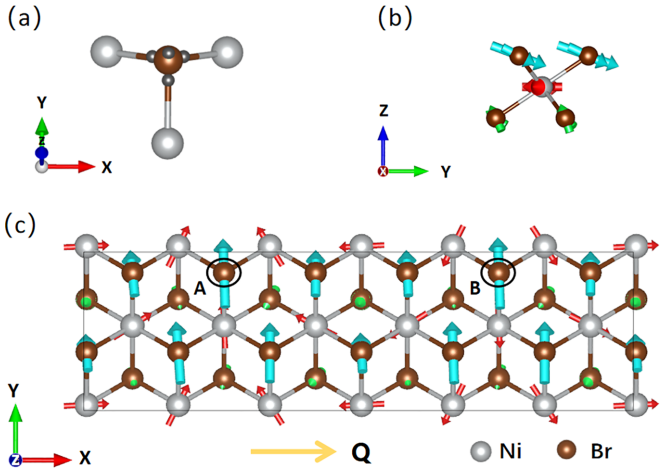

FIG. 4. (a) The positions of the centers of Wannier functions around one Br ion. (b) The side view and (c) the top view of the magnetic moments on Ni ions (red arrows) and the electric dipoles of Br ions (blue and green arrows) within a supercell with $q = 1/12$.

moments of Br ions oscillate by two periods. Taking two Br ions, highlighted by "A" and "B" in Fig. 4(c) as an example, the dipole moment of a Br ion remains the same when the magnetic moment of three adjacent Ni rotates by 180°. This result is consistent with our model and the OPENMX calculations. The analysis using Wannier function centers confirms that the Br atomic orbitals with strongly hybridized Ni orbitals are the major contributor to the electric polarization. This conclusion is consistent with the above OPENMX calculations.

IV. CONCLUSIONS

In this work, we performed first-principles calculations on the noncollinear spin induced ferroelectricity in monolayer $NiBr_2$. The calculated polarization is inversely proportional to the band gap of $NiBr_2$. Using an appropriate choice of the Hubbard correction, we have reproduced the experimental data of polarization and its linear dependence on the length of magnetic modulation vector. The spin-orbital coupling of Br sites, rather than Ni, play the dominating role in generating the electric dipole moment; The Br atomic orbitals are the major contributor to the electric polarization. Spin-induced atomic relaxations have a negligible effect on the polarization. This work paves the way for understanding the spin-induced ferroelectricity in transition-metal dihalides, such as NiI_2, MnI_2, CoI_2, and FeI_2.

ACKNOWLEDGMENTS

This work is supported by the National Natural Science Foundation of China (Grant No. 12004439), the Natural Science Foundation of Hunan Province (Grant No. 2022JJ30049), and the computational resources from the High Performance Computing Center of Central South University.

[1] D. Khomskii, Physics **2**, 20 (2009).
[2] Y. Tokura, S. Seki, and N. Nagaosa, Rep. Prog. Phys. **77**, 076501 (2014).
[3] C. Lu, M. Wu, L. Lin, and J.-M. Liu, Natl. Sci. Rev. **6**, 653 (2019).
[4] Y. Gao, M. Gao, and Y. Lu, Nanoscale **13**, 19324 (2021).
[5] H. Katsura, N. Nagaosa, and A. V. Balatsky, Phys. Rev. Lett. **95**, 057205 (2005).
[6] M. Mostovoy, Phys. Rev. Lett. **96**, 067601 (2006).
[7] C. Jia, S. Onoda, N. Nagaosa, and J. H. Han, Phys. Rev. B **74**, 224444 (2006).
[8] C. Jia, S. Onoda, N. Nagaosa, and J. H. Han, Phys. Rev. B **76**, 144424 (2007).
[9] H. Ju, Y. Lee, K.-T. Kim, I. H. Choi, C. J. Roh, S. Son, P. Park, J. H. Kim, T. S. Jung, J. H. Kim *et al.*, Nano Lett. **21**, 5126 (2021).
[10] Q. Song, C. A. Occhialini, E. Ergeçen, B. Ilyas, D. Amoroso, P. Barone, J. Kapeghian, K. Watanabe, T. Taniguchi, A. S. Botana *et al.*, Nature (London) **602**, 601 (2022).
[11] M. A. McGuire, Crystals **7**, 121 (2017).
[12] A. S. Botana and M. R. Norman, Phys. Rev. Mater. **3**, 044001 (2019).
[13] M. An and S. Dong, APL Mater. **8**, 110704 (2020).
[14] H. J. Xiang, E. J. Kan, Y. Zhang, M.-H. Whangbo, and X. G. Gong, Phys. Rev. Lett. **107**, 157202 (2011).
[15] X. Wu, Y. Cai, Q. Xie, H. Weng, H. Fan, and J. Hu, Phys. Rev. B **86**, 134413 (2012).
[16] A. O. Fumega and J. L. Lado, 2D Mater. **9**, 025010 (2022).
[17] Y. Tokunaga, D. Okuyama, T. Kurumaji, T. Arima, H. Nakao, Y. Murakami, Y. Taguchi, and Y. Tokura, Phys. Rev. B **84**, 060406(R) (2011).
[18] J. Y. Ni, X. Y. Li, D. Amoroso, X. He, J. S. Feng, E. J. Kan, S. Picozzi, and H. J. Xiang, Phys. Rev. Lett. **127**, 247204 (2021).
[19] G. Kresse and J. Hafner, Phys. Rev. B **47**, 558 (1993).
[20] G. Kresse and J. Hafner, Phys. Rev. B **49**, 14251 (1994).
[21] G. Kresse and J. Furthmüller, Phys. Rev. B **54**, 11169 (1996).
[22] G. Kresse and J. Furthmüller, Comput. Mater. Sci. **6**, 15 (1996).
[23] T. Ozaki, Phys. Rev. B **67**, 155108 (2003).
[24] T. Ozaki and H. Kino, Phys. Rev. B **69**, 195113 (2004).
[25] T. Ozaki and H. Kino, Phys. Rev. B **72**, 045121 (2005).
[26] A. I. Liechtenstein, V. I. Anisimov, and J. Zaanen, Phys. Rev. B **52**, R5467 (1995).
[27] S. L. Dudarev, G. A. Botton, S. Y. Savrasov, C. J. Humphreys, and A. P. Sutton, Phys. Rev. B **57**, 1505 (1998).
[28] R. D. King-Smith and D. Vanderbilt, Phys. Rev. B **47**, 1651 (1993).
[29] D. Vanderbilt and R. D. King-Smith, Phys. Rev. B **48**, 4442 (1993).
[30] R. Resta, Rev. Mod. Phys. **66**, 899 (1994).
[31] A. Mostofi, J. Yates, Y.-S. Lee, I. Souza, D. Vanderbilt, and N. Marzari, Comput. Phys. Commun. **178**, 685 (2008).
[32] See Supplemental Material at http://link.aps.org/supplemental/10.1103/PhysRevB.108.054429 for the details of the setup and results of the cluster model.